

Cost-Effective Single-Antenna RSSI Positioning Through Dynamic Radiation Pattern Analysis

Zhisheng Rong*, Wenzhi Liu*, Xiayue Liu, Zhixiang Xu,
Yufei Jiang, *Member, IEEE* Xu Zhu, *Senior Member, IEEE*,

Abstract—Mobile robot positioning systems traditionally rely on multiple antennas, increasing hardware complexity and cost. Thus, we propose a single-antenna positioning approach, where radiation pattern characteristics are leveraged based on maximum likelihood estimation (MLE) through received signal strength indication (RSSI) measurements. The proposed positioning approach is cost-effective, requiring only a single antenna. By rotating the antenna, we exploit asymmetric radiation patterns to achieve pattern diversity, which allows the single-antenna positioning system to approach the performance of multi-point positioning systems. We further propose a geometric-based curve intersection detection (CID) algorithm that outperforms conventional equation-solving methods. We theoretically derive the biased Cramér-Rao lower bound (CRLB) of the proposed positioning approach, dependent on signal-to-noise ratio (SNR), directivity of antenna radiation pattern and the number of rotation measurements. Simulation results show that all methods improve with increasing SNR, number of rotation and directivity of antenna radiation pattern, and the MLE achieves performance close to the derived biased CRLB.

Index Terms—RSSI positioning, antenna radiation pattern, single-antenna system, maximum likelihood estimation, Cramér-Rao lower bound

I. INTRODUCTION

Mobile robots play a crucial role in various fields, including industrial automation, smart logistics, emergency response, environmental monitoring, and healthcare [1]. Accurate positioning are critical for the effective operation of mobile robots. While Global Positioning System (GPS) and similar satellite-based technologies have transformed outdoor navigation, their positioning accuracy remains insufficient for robot location [2]. Current research in robotics has primarily relied on simultaneous localization and mapping (SLAM), which suffer from computational complexity and trajectory constraints [1]. Consequently, robot wireless positioning techniques have emerged as a promising research frontier to enhance mobile robot autonomy [2].

Among the various positioning techniques, technologies like Time of Flight (ToF), Angle of Arrival (AoA), Phase of Arrival (PoA), Received Signal Strength Indication (RSSI), and Channel State Information (CSI) have been extensively studied [3]. While each approach has its own limitations. ToF requires precise timing, AoA struggles with obstacles, PoA is noise-sensitive, and CSI demands extensive data processing. In contrast, RSSI stands out as a more practical option due to its simpler hardware requirements and easier integration with existing wireless systems, even though its positioning accuracy is relatively lower [4].

*These authors contributed equally to this work.

Many researchers have focused on improving the accuracy and applicability of RSSI for robot position. Approaches such as filtering algorithms and machine learning have been used to enhance positioning accuracy and reduce errors [5]. However, these methods often increase computational complexity, require large datasets, and introduce delays that impact real-time performance. As a result, RSSI is still primarily used as an auxiliary tool in robot position, such as distance estimation or database creation [6].

Newer approaches aim to expand RSSI's potential by addressing signal fluctuations at the transmitter side. For example, [7] proposed a positioning method that updates stored data with real-time RSSI values, changing the parameters to reduce the result error according to the fluctuation of the transmitter. Other studies challenge the assumption of omnidirectional antenna radiation patterns, considering the impact of radiation pattern on signal strength. Research has shown that antenna polarization and irregular radiation patterns affect positioning accuracy [8], and incorporating radiation pattern into positioning algorithms [9] or using positioning techniques based on radiation pattern [10] has led to improved accuracy. However, many of these studies analyze radiation pattern as a source of error, failing to fully exploit the additional information provided by them.

Building upon prior research, we develop a novel single-antenna positioning system, leveraging the inherent asymmetry of antenna radiation patterns. The positioning capability is realized by dynamically controlling antenna radiation pattern variations, implemented either via mechanical antenna rotation or reconfigurable antenna. Compared to conventional multi-antenna positioning systems, the proposed single-antenna approach offers notable advantages, including reduced hardware complexity and lowered design expenses, while preserving positioning accuracy. The main contributions of this paper are summarized as follows:

- We propose a localization scheme leveraging pattern diversity through antenna rotation, where asymmetric radiation patterns enable single-antenna systems to approach multi-antenna performance. Based on this approach, we derive a maximum likelihood estimation (MLE) positioning method that approaches the derived biased Cramér-Rao lower bound (CRLB), showing superior distance estimation but inferior angle estimation compared to multi-point systems.
- We establish a mathematical framework characterizing estimation accuracy bounds and analyze system performance. Our analysis reveals that positioning accuracy

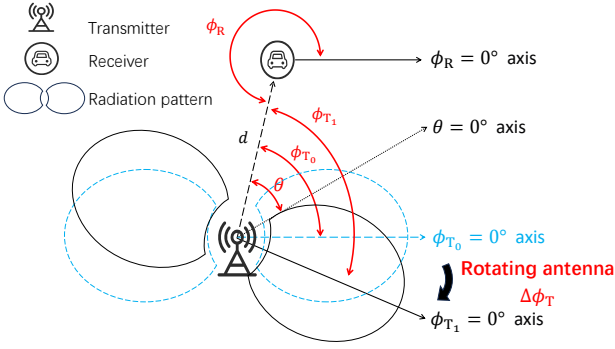


Fig. 1. System model for single-antenna positioning using pattern rotation, where d denotes transmitter-receiver distance, and θ represents the angle relative to the $\theta = 0^\circ$ axis. $\Delta\phi_T$ denotes the angle the axis changes from $\phi_{T_0} = 0^\circ$ to $\phi_{T_1} = 0^\circ$, indicating the antenna rotation. And ϕ_{T_i} represents the angle between the transmitter and receiver in the i -th transmitting antenna coordinate system relative to $\phi_{T_i} = 0^\circ$ axis, ϕ_R represents the angle in the receiving antenna coordinate system relative to its $\phi_R = 0^\circ$ axis.

improves with increased SNR, more antenna rotations, and steeper radiation pattern variations, providing essential design guidelines for practical implementation.

- We develop a generalized geometric algorithm called curve intersection detection (CID) for robust localization under both antenna rotation and reconfigurable pattern variations scenarios. This method achieves estimation accuracy closer to the CRLB compared to equation-solving approaches.

II. SYSTEM MODEL

Consider a robotic swarm communication, where each robotic equipped with a single antenna. This configuration is particularly relevant to the system consisting of a single transmitter and multiple receivers [1], [2], as shown in Fig.1.

In this paper, we assume the capability of rotating antenna radiation patterns through either mechanical rotation or electronic steering [11]. As shown in Fig.1, ϕ_{T_i} denotes the transmission angle measured from the transmitter's reference axis after the antenna has undergone i rotations, and ϕ_{T_0} denotes the the initial transmission angle before any rotation relative to $\phi_{T_0} = 0^\circ$ axis. ϕ_R denotes the reception angle measured from the receiver's reference axis, and θ represents the relative angle between transmitter and receiver. d denotes the distance between transmitter and receiver. The known angle of the transmitting antenna radiation pattern rotations is defined as $\Delta\phi_T$. For simplicity of expression, we align $\phi_{T_0} = 0^\circ$ axis with the $\theta = 0^\circ$ axis without loss of generality, thus

$$\phi_{T_0} = \theta, \quad \phi_{T_i} = \theta + \Delta\phi_T. \quad (1)$$

According to the Friis transmission equation [12] and considering the shadowing fading effects, the RSSI between transmitter and receiver positioned at (d, θ) relative to transmitter can be expressed as

$$\mathcal{R}(\phi_T, \phi_R)|_{(d, \theta)} = 10 \log_{10} \left(\frac{P_T \lambda^2 G_T(\phi_T) G_R(\phi_R)}{(4\pi)^2 d^n} \right) + 30 + X_\sigma, \quad (2)$$

where P_T denotes the transmission power, λ denotes the signal wavelength. $G_T(\phi_T)$ and $G_R(\phi_R)$ denote the antenna gains at the transmitter and receiver, respectively. The path loss exponent n characterizes the propagation environment, and is usually a number from 2 to 6 [13]. X_σ represents the shadowing effects, modeled as a zero-mean Gaussian random variable with variance σ^2 , i.e., $X_\sigma \sim \mathcal{N}(0, \sigma^2)$.

III. STATIONARY POSITIONING

To achieve RSSI-based positioning with a single antenna, we conducting theoretical analysis, leveraging the radiation pattern rotation capabilities of reconfigurable antennas. Subsection III-A analyzes the feasibility of this positioning approach with omnidirectional receiving antennas, featuring a MLE method along with comprehensive performance evaluation, and derives the biased CRLB. Subsection III-B extends this approach by applying two-position measurement strategy to address positioning challenges with directional receiving antennas.

A. Under Known Receiving Antenna Radiation Pattern

For a fixed receiving antenna at position (d_0, θ_0) with constant radiation pattern G_R , d_0 can be derived from (2)

$$d_0 = \sqrt[n]{A^2 G_T(\phi_T) G_R} \cdot 10^{-\frac{\mathcal{R}(\phi_T, \phi_R)|_{(d_0, \theta_0)} - 30 - X_\sigma}{10n}}. \quad (3)$$

where $A = \sqrt{\frac{P_T \lambda^2}{(4\pi)^2}}$. This formulation yields a system of coupled equations in d_0 and ϕ_T .

To solve this coupled system, we rotate the transmitting antenna through different angles $[\phi_{T_0}, \phi_{T_1}, \dots, \phi_{T_N}]$ which provides a sequence of signal strength measurements $[R(\phi_{T_0}), R(\phi_{T_1}), \dots, R(\phi_{T_N})]$ given by:

$$R(\phi_{T_i}) = 10 \cdot \log_{10} \left(A^2 \frac{G_T(\phi_{T_i}) G_R}{d_0^n} \right) + 30 + X_{\sigma_i}, \quad (4)$$

where $X_{\sigma_i} \sim \mathcal{N}(0, \sigma^2)$. Since $M_i(d, \theta) = 30 + 10n \cdot \log_{10} \left(\frac{\sqrt[n]{A^2 G_T(\theta + \Delta\phi_T) G_R}}{d_0} \right)$ is a constant, $R(\phi_{T_i})$ is a Gaussian variable with mean $M_i(d, \theta)$ and variance σ^2 , i.e.

$$R(\phi_{T_i}) \sim \mathcal{N}(M_i(d, \theta), \sigma^2). \quad (5)$$

Since the angular differences between antenna pattern rotations $[\Delta\phi_{T_1}, \Delta\phi_{T_2}, \dots, \Delta\phi_{T_N}]$ are known, we can propose N equations from (3):

$$d_0 = \sqrt[n]{A^2 G_T(\theta_0 + \Delta\phi_{T_i}) \cdot G_R} \cdot 10^{-\frac{R(\phi_{T_i}) - 30 - X_{\sigma_i}}{10n}} \quad (6)$$

where $\Delta\phi_{T_i} = \phi_{T_i} - \phi_{T_0}$, and i from 1 to N .

d_0 and θ_0 can be determined by solving the system of equations (6), though the nonlinear solution process incurs significant computational cost. Then a Curve Intersection Detection Algorithm, **Algorithm 1**, is proposed to determine d and θ efficiently. This algorithm identifies critical intersection points of distinct function curves, where each curve comes from the equation in (6) and has the form shown in (3) with respect to ϕ_T . Therefore, these intersection points represent the solutions to the corresponding equations. This method avoids the complex nonlinear system solving process, and is

Algorithm 1 Curve Intersection Detection (CID)

Input: $n_t, P_t, G_t, G_r, d_0, \theta_0$;

Execute:

- 1: **for** $i = 1$ **to** N **do**
 - 2: Given $R(\phi_{T_i})$ is obtained by (4);
 - 3: Given target curve $d(\theta)|_{\phi_T=\phi_{T_i}}$ is obtained by (6);
 - 4: **end for**
 - 5: Given $(d, \theta)_{ij}$ is obtained from the intersection points of the curves $d(\theta)|_{\phi_T=\phi_{T_i}, \phi_{T_j}}$;
 - 6: Given $(\hat{d}, \hat{\theta})$ is obtained from the average value of $(d, \theta)_{ij}$;
 - 7: **return** $(\hat{d}, \hat{\theta})$;
-

applicable to both antenna rotation and reconfigurable antenna pattern variations since (3) imposes no constraints on antenna radiation patterns.

For the case of antenna rotation, the radiation pattern remains consistent across all angular positions. We propose an estimator based on the MLE methodology to improve both computational efficiency and estimation accuracy.

Given the observation $R(\phi_{T_i})$ to estimate its probability density function, the log-likelihood function $L(d, \theta)$ is defined as

$$\ln(L(d, \theta)) = -\frac{N}{2} \ln(2\pi\sigma^2) - \frac{1}{2\sigma^2} \sum_{i=1}^N [R(\phi_{T_i}) - M_i(d, \theta)]^2. \quad (7)$$

The optimal parameters $(\hat{d}, \hat{\theta})$ can be determined by maximizing the log-likelihood function $\ln(L(d, \theta))$, i.e.,

$$(\hat{d}, \hat{\theta}) = \arg \max_{(d, \theta)} \ln(L(d, \theta)). \quad (8)$$

To obtain the optimal values of $(\hat{d}, \hat{\theta})$ that maximize $\ln(L(d, \theta))$, we solve the following system of equations

$$\frac{\partial \ln L(d, \theta)}{\partial d} = \sum_{i=1}^N \left([R(\phi_{T_i}) - M_i(\hat{d}, \hat{\theta})] \frac{\partial M_i(d, \theta)}{\partial d} \right) = 0 \quad (9)$$

$$\frac{\partial \ln L(d, \theta)}{\partial \theta} = \sum_{i=1}^N \left([R(\phi_{T_i}) - M_i(\hat{d}, \hat{\theta})] \frac{\partial M_i(d, \theta)}{\partial \theta} \right) = 0, \quad (10)$$

\hat{d} and $\hat{\theta}$ can be solved from the nonlinear equations (9)(10).

Proposition 1: The distance estimator \hat{d} (11) is biased. The bias level increases with noise intensity σ^2 and angular estimation $\hat{\theta}$, while decreasing with the number of measurements N .

$$\hat{d} = d_0 \cdot 10^{\frac{X'_\sigma}{10n \cdot N}} \cdot \left(\prod_{i=1}^N \Gamma_i(\hat{\theta}) \right)^{\frac{1}{n \cdot N}}, \quad (11)$$

where $X'_\sigma = -\sum_{i=1}^N X_{\sigma_i}$, $\Gamma_i(\hat{\theta}) = \frac{G_T(\hat{\theta} + \Delta\phi_{T_i})}{G_T(\theta_0 + \Delta\phi_{T_i})}$. Notably, the distance estimate maintains its bias even when the angular estimator $\hat{\theta}$ is unbiased. This persistent bias stems from the inherent properties of the log-normal distribution, specifically that its mean value deviates from unity.

Proof: See Appendix A ■

Proposition 2: The angular estimator $\hat{\theta}$ solved by (12) is independent of the distance parameter d , :

$$10n \log_{10} \left(\prod_{i=1}^N \Gamma_i(\hat{\theta})^{\frac{\mathcal{H} - N \cdot K_i}{n \cdot N}} \right) + \sum_{i=1}^N (K_i - \frac{\mathcal{H}}{N}) X_{\sigma_i} = 0. \quad (12)$$

where $K_i = \frac{10}{\ln 10} \cdot \frac{G'_T(\hat{\theta} + \Delta\phi_{T_i})}{G_T(\hat{\theta} + \Delta\phi_{T_i})}$, $\mathcal{H} = \sum_{i=1}^N K_i$.

Proof: See Appendix B

Remark 1: Furthermore, the accuracy of angular estimation improves with increasing variance of the sequence $\{\frac{G'_T(\theta + \Delta\phi_{T_i})}{G_T(\theta + \Delta\phi_{T_i})}\}_{i=1}^N$, denoted as \mathcal{G} . A larger variance of \mathcal{G} indicates increased directivity in the antenna radiation pattern. ■

Proposition 3: The CRLB for biased distance estimation \hat{d} and angular estimation $\hat{\theta}$ is derived as:

$$\text{CRLB}([\hat{d}, \hat{\theta}]) = \begin{bmatrix} \beta_d^2 & \beta_d \beta_\theta \\ \beta_d \beta_\theta & \beta_\theta^2 \end{bmatrix} + \begin{bmatrix} \frac{\partial \beta_d}{\partial d} & \frac{\partial \beta_d}{\partial \theta} \\ \frac{\partial \beta_\theta}{\partial d} & \frac{\partial \beta_\theta}{\partial \theta} \end{bmatrix} \mathbf{J}_D^{-1} \begin{bmatrix} \frac{\partial \beta_d}{\partial d} & \frac{\partial \beta_d}{\partial \theta} \\ \frac{\partial \beta_\theta}{\partial d} & \frac{\partial \beta_\theta}{\partial \theta} \end{bmatrix}, \quad (13)$$

where:

$$\mathbf{J}_D^{-1} = \begin{bmatrix} \mathbf{J}_{D,1,1}^{-1} & \mathbf{J}_{D,1,2}^{-1} \\ \mathbf{J}_{D,2,1}^{-1} & \mathbf{J}_{D,2,2}^{-1} \end{bmatrix},$$

$$[\mathbf{J}_D^{-1}]_{1,1} = \frac{\frac{\sigma^2 d^2 \ln^2 10}{100n^2} \cdot \sum_{i=1}^N K_i^2}{N \cdot \sum_{i=1}^N K_i^2 - \left(\sum_{i=1}^N K_i \right)^2}, \quad (14)$$

$$[\mathbf{J}_D^{-1}]_{2,2} = \frac{N\sigma^2}{N \cdot \sum_{i=1}^N K_i^2 - \left(\sum_{i=1}^N K_i \right)^2}, \quad (15)$$

$$[\mathbf{J}_D^{-1}]_{1,2} = [\mathbf{J}_D^{-1}]_{2,1} = \frac{\frac{\sigma^2 d \ln 10}{10n} \cdot \sum_{i=1}^N K_i^2}{N \cdot \sum_{i=1}^N K_i^2 - \left(\sum_{i=1}^N K_i \right)^2}. \quad (16)$$

Proof: See Appendix C ■

Remark 2: Based on (14) and (15), we deduce that $\text{CRLB}(\hat{d})$ increases with noise intensity σ^2 and distance parameter d , while decreasing with the number of measurements N . Conversely, $\text{CRLB}(\hat{\theta})$ increases with σ^2 and decreases with N , but remains unaffected by d . And for high signal-to-noise ratio (SNR) scenarios, where the estimates of \hat{d} and $\hat{\theta}$ exhibit negligible bias, we derive the lower bound for the mean squared errors which are expressed as $\text{MSE}(\hat{d})$ and $\text{MSE}(\hat{\theta})$

$$\text{MSE}(\hat{d}) \geq [\mathbf{J}_D^{-1}]_{1,1}, \text{MSE}(\hat{\theta}) \geq [\mathbf{J}_D^{-1}]_{2,2}. \quad (17)$$

B. Under Unknown Receiving Antenna Radiation Pattern

While Subsection III-A addresses position estimation with known antenna radiation patterns, practical scenarios often encounter unknown receiving antenna patterns $G_R(\phi_R)$, necessitating an enhanced positioning strategy.

We eliminate the dependence on $G_R(\phi_R)$ by exploiting the differential RSSI measurements between two distinct angles. From (2), this relationship is expressed as:

$$\mathcal{R}(\phi_{T_1}, \phi_R) - \mathcal{R}(\phi_{T_2}, \phi_R) = 10 \log_{10} \left(\frac{G_T(\phi_{T_1})}{G_T(\phi_{T_2})} \right) + X_{\sigma_1} - X_{\sigma_2}. \quad (18)$$

Algorithm 2 Angular Similarity-Based Localization

Input: $n_t, P_t, G_t, G_r, d_0, \theta_0$;

Execute:

- 1: **for** $i = 1$ **to** N **do**
 - 2: Given $\mathcal{R}(\phi_T, \phi_R)|_{(d_0, \theta_0)}$ is obtained by (2);
 - 3: Given $r(\phi_T)$ is obtained by (19);
 - 4: **end for**
 - 5: Given $\hat{\theta}$ is obtained from the similarity estimation between the curves $r(\phi_T)$ and $\frac{G_T(\theta + \Delta\phi_T)}{G_T(\theta)}$;
 - 6: Given \hat{d} is obtained by (3)
 - 7: **return** $(\hat{d}, \hat{\theta})$;
-

This formulation reveals that the RSSI differential corresponds to the transmitting antenna gain ratio. We characterize this relationship by varying ϕ_T ,

$$r(\phi_T) = 10^{\frac{1}{10}(\mathcal{R}(\theta_0 + \Delta\phi_T, \phi_R) - \mathcal{R}(\theta_0, \phi_R))} \quad (19)$$

$$= \frac{G_T(\theta_0 + \Delta\phi_T)}{G_T(\theta_0)} \cdot 10^{\frac{x_{\sigma_2} - x_{\sigma_1}}{10}}. \quad (20)$$

The initial angle θ_0 is estimated by correlating the measured curve with the known normalized transmitting radiation pattern $\frac{G_T(\theta_0 + \phi_T)}{G_T(\theta_0)}$.

We employ similarity analysis as detailed in **Algorithm 2** to determine the object's direction θ_0 to mitigate the effects of noise and potential reference gain misalignment. And a two-position measurement strategy is used in order to overcome the unknown receiving antenna gain problem. After removing the transmitting antenna by a distance m and obtaining a second angular measurement θ_1 of receiving antenna, geometric relationships yield:

$$d_0 = \frac{\sin(\theta_1) \cdot m}{\sin(\theta_1 - \theta_0)}, d_1 = \frac{\sin(\theta_0) \cdot m}{\sin(\theta_1 - \theta_0)}. \quad (21)$$

IV. SIMULATION RESULTS

A. Simulation Setup

In this section, we conduct numerical simulations to verify the theoretical analysis and the proposed algorithms. We model a half-dipole antenna as the transmitting antenna and operate in a 2D plane to satisfy directional pattern requirements. The path loss exponent in the Friis equation is $n = 4$ to emulate indoor environments. The transmission parameters are configured with $P_T = 100$ mW and $\lambda = 125$ mm. An omnidirectional antenna with gain $G_R = 0$ dB serves as the receiving antenna, deployed within the range of 0.5 - 5 m and -70° to 70° . The scenario settings in Figs. 2(a), 2(b) are as follows: the transmitter rotation count is $N = 8$ with a step angle of $\Delta\phi_T = 4^\circ$, while the SNR varies from 0 to 20 dB. The scenario settings in Figs. 3(a), 3(b) are as follows: SNR = 10 dB, $\Delta\phi_T = 3^\circ$, while N varies from = 5 to 14. And in Fig. 4(b): SNR = 10 dB, $N = 8$, while $\Delta\phi_T$ varies from 1° to 10° to analysis the effects of \mathcal{G} variance.

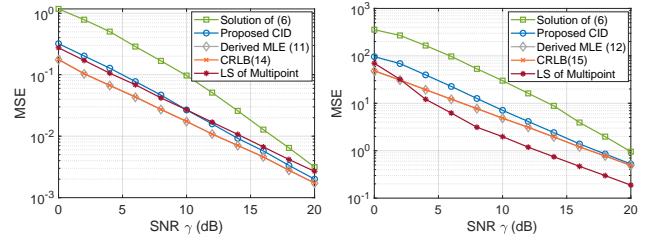
(a) Distance estimation d (b) Angle estimation θ

Fig. 2. Performance comparison between different estimation methods and CRLB with $N = 8$ measurements, $\Delta\phi_T = 4^\circ$.

B. Estimation Accuracy Comparison

We evaluate the positioning performance by analyzing the mean square error (MSE) of the estimates under various operational conditions.

Figs. 2(a) and 2(b) illustrate the MSE performance versus SNR for distance and angle estimation, respectively. The performance of all methods improves with increasing SNR, with the solution of (6) showing the poorest performance. The proposed CID algorithm demonstrates improved accuracy, while the derived MLE achieves near-optimal performance by approaching the theoretical CRLB. Compared to multi-point localization methods, our approach demonstrates superior distance estimation while exhibiting lower angular estimation performance. This performance difference stems from the inherent characteristics of our pattern diversity approach. In our system, distance estimation benefits from measurement redundancy as the actual distance remains invariant across different antenna orientations, while each radiation pattern provides an independent signal strength sample. Conversely, angular information is embedded within the relative differences between radiation patterns and obtained through indirect derivation.

The effect of antenna rotation count on estimation accuracy is examined in Figs. 3(a) and 3(b). Results show enhanced performance for all methods as N increases from 7 to 14, with the MLE maintaining near-CRLB performance throughout. These experimental results validate our theoretical analysis **Propositions 1 and 2**, confirming the positive correlation between estimation accuracy and both SNR and measurement count.

Figs. 4(a) and 4(b) examine the relationship between distance and angular estimation performance and the variance of \mathcal{G} to quantify the impact of antenna radiation patterns. The results reveal that larger variance in \mathcal{G} leads to improved estimation accuracy for all methods, which validates the theoretical analysis in **Propositions 2**.

V. CONCLUSION

In this paper, we presented a cost-effective positioning approach leveraging antenna radiation pattern characteristics based on RSSI and proposed corresponding algorithms. Through antenna rotation, we leverages asymmetric radiation patterns to achieve pattern diversity. Based on this system,

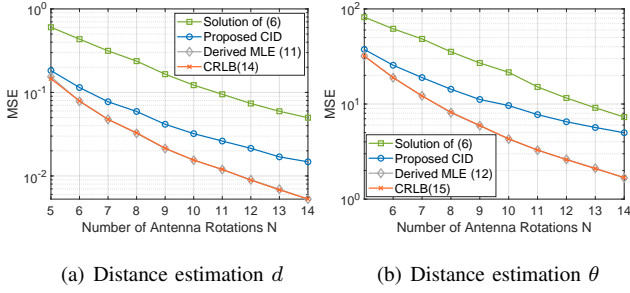


Fig. 3. Performance comparison between different estimation methods and CRLB with SNR = 10 dB, $\Delta\phi_T = 3^\circ$.

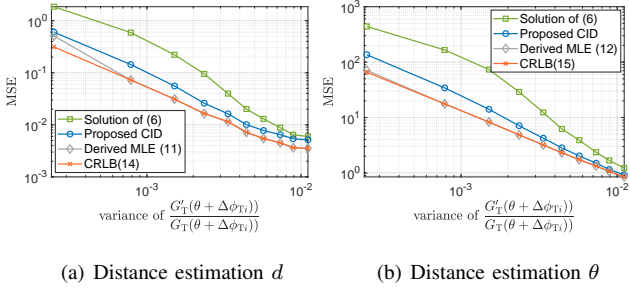


Fig. 4. Estimation variance for distance \hat{d} and angle $\hat{\theta}$ versus variance of \mathcal{G} with SNR = 10 dB, $N = 8$ measurements.

we make theoretical analysis and simulations, established three fundamental proposition characterizing the estimation accuracy bounds. Our simulations demonstrates that the derived MLE method achieves near-optimal performance by approaching the CRLB. The proposed CID algorithm demonstrates robust performance across diverse antenna configurations, including both mechanical rotation and electronically reconfigurable patterns. The experimental results validate our theoretical findings that estimation accuracy improves with increased SNR, antenna rotation count, and steeper variations in the antenna radiation pattern. And compared to multi-point localization methods, our approach demonstrates superior distance estimation while exhibiting lower angular estimation performance. To enhance practical applicability, we developed a two-position measurement strategy that eliminates dependence on receiving antenna patterns while maintaining positioning accuracy. This approach provides a promising solution for indoor robot position applications where both accuracy and system simplicity are essential considerations.

APPENDIX A PROOF OF PROPOSITION 1

Owing to $\frac{\partial M_i(d, \theta)}{\partial d} = \frac{-10n}{d \ln 10}$ is a constant independent of i and not equal to zero, (9) is equivalent to

$$\sum_{i=1}^N R(\phi_{T_i}) - \sum_{i=1}^N M_i(\hat{d}, \hat{\theta}) = 0. \quad (22)$$

By substituting (4) into (22):

$$\frac{\hat{d}^N}{\prod_{i=1}^N \sqrt{n A^2 G_T(\hat{\theta} + \Delta\phi_{T_i}) G_R}} = \frac{d_0^N \cdot \frac{1}{10n} X'_\sigma}{\prod_{i=1}^N \sqrt{n A^2 G_T(\theta_0 + \Delta\phi_{T_i}) G_R}}. \quad (23)$$

$$\hat{d} = d_0 \cdot 10^{\frac{1}{10n \cdot N} X'_\sigma} \cdot \left(\prod_{i=1}^N \Gamma(\hat{\theta}) \right)^{\frac{1}{n \cdot N}}. \quad (24)$$

When $\hat{\theta} = \theta_0$, the expression simplifies to $\hat{d} = d_0 \cdot 10^{\frac{1}{10n \cdot N} X'_\sigma}$, yielding $\log_{10} \hat{d} = \log_{10} d_0 + \frac{1}{10n \cdot N} X'_\sigma$. Consequently, $\log_{10} \hat{d}$ follows a normal distribution: $\log_{10} \hat{d} \sim \mathcal{N}\left(\log_{10} d_0, \frac{\sigma^2}{100n^2 \cdot N}\right)$. Through the probability density transformation theorem, it can be concluded that

$$f_{\hat{d}}(h) = f_{\log_{10} \hat{d}}(\log_{10} h) \cdot \left| \frac{d(\log_{10} h)}{dh} \right| \quad (25)$$

$$= \frac{10n \cdot \sqrt{N}}{\sigma h (\ln 10) \sqrt{2\pi}} e^{-\frac{50n^2 \cdot N (\log_{10} h - \log_{10} d_0)^2}{\sigma^2}}. \quad (26)$$

Then:

$$E[\hat{d}] = \int_0^{+\infty} \frac{10n \cdot \sqrt{N}}{\sigma (\ln 10) \sqrt{2\pi}} e^{-\frac{50n^2 \cdot N (\log_{10} h - \log_{10} d_0)^2}{\sigma^2}} dh \quad (27)$$

$$\stackrel{(a)}{=} \frac{d_0}{\sqrt{2\pi}} \int_{-\infty}^{+\infty} e^{-\frac{1}{2} t^2 + \frac{\sigma}{10n} t \cdot \ln 10} dt \quad (28)$$

$$= \frac{d_0 \cdot e^{\frac{1}{2} \left(\frac{\sigma}{10n \cdot \sqrt{N}} \ln 10 \right)^2}}{\sqrt{2\pi}} \int_{-\infty}^{+\infty} e^{-\frac{1}{2} \left(t - \frac{\sigma}{10n} \ln 10 \right)^2} dt \quad (29)$$

$$= d_0 \cdot 10^{\frac{\sigma^2}{200n^2 \cdot N} \ln 10}. \quad (30)$$

where (a) represents: $t = \frac{10n \cdot \sqrt{N} (\log_{10} h - \log_{10} d_0)}{\sigma}$.

APPENDIX B PROOF OF PROPOSITION 2

Let $\frac{\partial M_i(d, \theta)}{\partial \theta} \Big|_{\theta=\hat{\theta}} = \frac{10}{\ln 10} \cdot \frac{G'_T(\hat{\theta} + \Delta\phi_{T_i})}{G_T(\hat{\theta} + \Delta\phi_{T_i})}$ be abbreviated as K_i , $\sum_{i=1}^N K_i$ be abbreviated as \mathcal{H} and $\frac{G_T(\hat{\theta} + \Delta\phi_{T_i})}{G_T(\theta_0 + \Delta\phi_{T_i})}$ be abbreviated as $\Gamma_i(\hat{\theta})$. Substituting the expression of $R(\phi_{T_i})$, $M_i(d, \theta)$ into (10), we have

$$\sum_{i=1}^N 10n \cdot \log_{10} \left(\frac{\hat{d}}{d_0} \cdot \sqrt[n]{\frac{1}{\Gamma_i(\hat{\theta})}} \right)^{K_i} + K_i X_{\sigma_i} = 0. \quad (31)$$

By applying the logarithmic addition rule, (31) simplifies to

$$10n \cdot \log_{10} \left(\left(\frac{\hat{d}}{d_0} \right)^{\mathcal{H}} \cdot \prod_{i=1}^N \Gamma_i(\hat{\theta})^{-\frac{K_i}{n}} \right) + K_i X_{\sigma_i} = 0. \quad (32)$$

Substituting (11) into (32), we obtain

$$10n \log_{10} \left(\prod_{i=1}^N \Gamma_i(\hat{\theta})^{\frac{\mathcal{H} - N \cdot K_i}{n \cdot N}} \right) + \sum_{i=1}^N \left(K_i - \frac{\mathcal{H}}{N} \right) X_{\sigma_i} = 0. \quad (33)$$

$\Gamma_i(\hat{\theta}) \neq 1$ when the estimated angle differs from its true value ($\hat{\theta} \neq \theta_0$). Due to the monotonic nature of the exponential function, the estimation bias magnitude is characterized by $\left| \frac{\mathcal{H}}{n \cdot N} - \frac{K_i}{n} \right|$. This term corresponds to the variance of K_i , indicating that increased variance of \mathcal{G} enhances the system's sensitivity to estimation errors.

APPENDIX C
PROOF OF PROPOSITION 3

Considering the bias in distance estimation, the calculation of the CRLB for this method requires the use of the following formula from [14]

$$E_R [(\hat{\alpha}(\mathbf{R}) - \alpha)(\hat{\alpha}(\mathbf{R}) - \alpha)^T] \geq \beta(\alpha)\beta(\alpha)^T + \frac{\partial E_R[\hat{\alpha}(\mathbf{R})]}{\partial \alpha^T} \mathbf{J}_D^{-1}(\alpha) \frac{\partial E_R[\hat{\alpha}(\mathbf{R})]}{\partial \alpha}, \quad (34)$$

where $\alpha = [d, \theta]^T$ denotes the parameter vector to be estimated, $\hat{\alpha} = [\hat{d}, \hat{\theta}]^T$ as the parameter estimate, $\mathbf{R} = [R(\phi_{T_0}), R(\phi_{T_1}) \dots R(\phi_{T_N})]$ as the random observation vector characterized by a conditional probability density function $p(\mathbf{R}; \alpha)$ which is equal to $\mathcal{L}(d, \theta)$. And $\beta(\alpha) = E_R[\hat{\alpha}(\mathbf{R}) - \alpha]$ is defined as the estimation error. $\mathbf{J}_D(\alpha)$ is the Fisher Information Matrix (FIM) given by:

$$\mathbf{J}_D(\alpha) = -E_R \left[\frac{\partial}{\partial \alpha} \ln p(\mathbf{R}; \alpha) \frac{\partial}{\partial \alpha^T} \ln p(\mathbf{R}; \alpha) \right]. \quad (35)$$

According to (35), given the Gaussian observations, elements of the FIM are derived as

$$[\mathbf{J}_D]_{1,1} = -E_R \left[\frac{\partial^2 \ln L(\mathbf{R}; d, \theta)}{\partial d^2} \right] = \frac{100n^2 \cdot N}{\sigma^2 \cdot (d \ln 10)^2}, \quad (36)$$

$$[\mathbf{J}_D]_{1,2} = [\mathbf{J}_D]_{2,1} = -E_R \left[\frac{\partial^2 \ln L(\mathbf{R}; d, \theta)}{\partial d \partial \theta} \right] = \frac{1}{\sigma^2} \sum_{i=1}^N \frac{-10n}{d \cdot \ln 10} \cdot K_i, \quad (37)$$

$$[\mathbf{J}_D]_{2,2} = -E_R \left[\frac{\partial^2 \ln L(\mathbf{R}; d, \theta)}{\partial \theta^2} \right] = \frac{1}{\sigma^2} \sum_{i=1}^N K_i^2. \quad (38)$$

By applying matrix inverse, we obtain

$$[\mathbf{J}_D^{-1}]_{1,1} = \frac{[\mathbf{J}_D]_{2,2}}{[\mathbf{J}_D]_{1,1}[\mathbf{J}_D]_{2,2} - [\mathbf{J}_D]_{1,2}^2} = \frac{\frac{\sigma^2 d^2 \ln^2 10}{100n^2} \cdot \sum_{i=1}^N K_i^2}{N \cdot \sum_{i=1}^N K_i^2 - \left(\sum_{i=1}^N K_i \right)^2}, \quad (39)$$

$$[\mathbf{J}_D^{-1}]_{2,2} = \frac{[\mathbf{J}_D]_{1,1}}{[\mathbf{J}_D]_{1,1}[\mathbf{J}_D]_{2,2} - [\mathbf{J}_D]_{1,2}^2} = \frac{N}{N \cdot \sum_{i=1}^N K_i^2 - \left(\sum_{i=1}^N K_i \right)^2}, \quad (40)$$

$$[\mathbf{J}_D^{-1}]_{1,2} = [\mathbf{J}_D^{-1}]_{2,1} = \frac{-[\mathbf{J}_D]_{1,2}}{[\mathbf{J}_D]_{1,1}[\mathbf{J}_D]_{2,2} - [\mathbf{J}_D]_{1,2}^2} = \frac{\frac{\sigma^2 d \ln 10}{10n} \cdot \sum_{i=1}^N K_i^2}{N \cdot \sum_{i=1}^N K_i^2 - \left(\sum_{i=1}^N K_i \right)^2}. \quad (41)$$

Then leveraging the distance estimation formulation (11), we have:

$$\beta_d = E \left(d \cdot 10^{\frac{1}{10n \cdot N}} X'_\sigma \cdot \left(\prod_{i=1}^N \Gamma(\hat{\theta}) \right)^{\frac{1}{n \cdot N}} - d \right), \quad (42)$$

$$\frac{\partial \beta_d}{\partial d} = E \left(10^{\frac{1}{10n \cdot N}} X'_\sigma \cdot \left(\prod_{i=1}^N \Gamma(\hat{\theta}) \right)^{\frac{1}{n \cdot N}} - 1 \right), \quad (43)$$

$$\frac{\partial \beta_d}{\partial \theta} = d \cdot E \left(10^{\frac{1}{10n \cdot N}} X'_\sigma \cdot \frac{\partial \left(\prod_{i=1}^N \Gamma(\hat{\theta}) \right)^{\frac{1}{n \cdot N}}}{\partial \theta} \right). \quad (44)$$

REFERENCES

- [1] I. Ullah, D. Adhikari, H. Khan *et al.*, "Mobile robot localization: Current challenges and future prospective," *Computer Science Review*, vol. 53, p. 100651, Aug. 2024.
- [2] P. S. Farahsari, A. Farahzadi, J. Rezazadeh *et al.*, "A survey on indoor positioning systems for iot-based applications," *IEEE Internet of Things Journal*, vol. 9, no. 10, pp. 7680–7699, Feb. 2022.
- [3] X. Mu, Y. Liu, L. Guo *et al.*, "Intelligent reflecting surface enhanced indoor robot path planning: A radio map-based approach," *IEEE Transactions on Wireless Communications*, vol. 20, no. 7, pp. 4732–4747, Mar. 2021.
- [4] P. Singh, N. Mittal, and R. Salgotra, "Comparison of range-based versus range-free wsns localization using adaptive ssa algorithm," *Wireless Networks*, vol. 28, no. 4, pp. 1625–1647, Mar. 2022.
- [5] M. T. Hoang, B. Yuen, X. Dong *et al.*, "Recurrent neural networks for accurate rssi indoor localization," *IEEE Internet of Things Journal*, vol. 6, no. 6, pp. 10639–10651, Sep. 2019.
- [6] H. Yucel, G. Elibol, and U. Yayan, "Wi-fi based indoor positioning system for mobile robots by using particle filter," *arXiv preprint arXiv:2012.05286*, Dec. 2020.
- [7] G. Li, E. Geng, Z. Ye *et al.*, "An indoor positioning algorithm based on rssi real-time correction," in *2018 14th IEEE International Conference on Signal Processing (ICSP)*. IEEE, Feb. 2018, pp. 129–133.
- [8] S. J. Maeng, H. Kwon, O. Ozdemir *et al.*, "Impact of 3d antenna radiation pattern in uav air-to-ground path loss modeling and rssi-based localization in rural area," *IEEE Open Journal of Antennas and Propagation*, Oct. 2023.
- [9] M. K. Mwila, K. Djouani, and A. Kurien, "The use of antenna radiation pattern in node localisation algorithms for wireless sensor networks," in *2014 International Wireless Communications and Mobile Computing Conference (IWCMC)*. IEEE, Sep. 2014, pp. 856–862.
- [10] L. Wang, L. Feng, and M. J. Zawodniok, "Arpap: A novel antenna-radiation-pattern-aware power-based positioning in rf system," *IEEE Transactions on Mobile Computing*, vol. 20, no. 3, pp. 816–829, Dec. 2019.
- [11] Y. Zhang, Z. Han, S. Tang *et al.*, "A highly pattern-reconfigurable planar antenna with 360° single- and multi-beam steering," *IEEE Transactions on Antennas and Propagation*, vol. 70, no. 8, pp. 6490–6504, 2022.
- [12] J. A. Shaw, "Radiometry and the friis transmission equation," *American journal of physics*, vol. 81, no. 1, pp. 33–37, 2013.
- [13] T. S. Rappaport, *Wireless communications: principles and practice*. Cambridge University Press, 2024.
- [14] D. H. Johnson and D. E. Dudgeon, *Array Signal Processing: Concepts and Techniques*. USA: Simon & Schuster, Inc., 1992.